`Letter of Intent for an experiment at PSI` R-98-05.0

Search for the decay $\mu^+ \to e^+\gamma$

with a branching-ratio sensitivity of 10^{-14}

JINR-KEK-Pavia-Pisa-PSI-Roma-Swierk-Tbilisi-Tokyo-Waseda-Zurich Collaboration

represented by:

Spartak Korenchenko spartak@axnua.jinr.dubna.su
JINR, Dubna, Russia

Yoshitaka Kuno kuno@tiempo.kek.jp and Akihiro Maki maki@kekvax.kek.jp
Institute of Particle and Nuclear Studies, KEK, Japan

Giacomo Bressi bressi@pv.infn.it
INFN, Pavia, Italy

Alessandro Baldini baldini@pi.infn.it and Carlo Bemporad bemporad@pi.infn.it
University of Pisa and INFN, Pisa, Italy

Fereydoun Foroughi foroughi@psi.ch, Dieter Renker renker@psi.ch and H.Christian Walter walter@psi.ch
PSI, CH-5232 Villigen PSI, Switzerland

Dino Zanello zanellos@roma1.infn.it
INFN, Roma1, IT-00185 Roma, Italy

Tadek Kozlowski p02tk@cx1.cyf.gov.pl and Marek Moszynski marek@sunp3.cyf.gov.pl
IPJ, PL 05-400 Otwock-Swierk, Poland

David Mzavia mzavia@sun20.hepi.edu.ge
HEPI, Tbilisi State University, GE-380086 Tbilisi, Georgia

Tetsuro Mashimo mashimo@icepp.s.u-tokyo.ac.jp, Toshinori Mori mori@icepp.s.u-tokyo.ac.jp and Shuji Orito oriton@icepp.s.u-tokyo.ac.jp
ICEPP, University of Tokyo, Tokyo, Japan

Tadayoshi Doke tdoke@mn.waseda.ac.jp and Jun Kikuchi jkikuchi@mn.waseda.ac.jp
Waseda University, Tokyo, Japan

Andries van der Schaaf * vanderschaaf@psi.ch
Physics Institute, University of Zurich, Switzerland

We intend to perform an experimental search for the decay $\mu^+ \to e^+\gamma$ which does not conserve lepton-flavor. It is our aim to reach a single-event sensitivity below 10^{-14}, which would improve on the previous result by 2–3 orders of magnitude. Various alternative techniques, both for the positron spectrometer and for the photon calorimeter, are presented.

---

*contactperson

Contents

I. INTRODUCTION

The non-observation of the decay $\mu \to e\gamma$ is one of the corner stones of the Standard Model. This test of lepton-flavor conservation is of similar importance as the limits on neutrino masses and mixings, proton stability, neutron electric dipole moment, and (g-2)$_{\mu,e}$. Each of them gives the best constraint to some varieties of extensions to the model. Each of them thus may give the first signal for physics beyond the Standard Model.

One of the great mysteries in present-day particle physics is the origin of the generation pattern of quark and lepton states. Transitions between the generations, as observed in charged weak interactions among quarks, can be attributed to mixing of the quark eigenstates. Within the framework of the minimal Standard Model the mass degeneracy of the neutrino states precludes this mechanism in the leptonic sector, in accordance with the apparent conservation of leptonic generation number (lepton-flavor conservation, LFC).

Although various anomalies in the fluxes of solar, atmospheric and beam dump neutrinos may be interpreted in terms of neutrino oscillations, no convincing signal for the violation of LFC has been found so far. Searches for LFC-violating decay modes of charged leptons, mesons and Z^0 have resulted in upper limits only.

Most extensions of the Standard Model allow neutral interactions between the generations. Whereas higher order charged interactions among quarks lead to effective flavor-changing neutral currents (FCNC), as observed in the decay $b \to s\gamma$, FCNC's among leptons would yield an unambiguous signal for new physics: neutrino mixing may contribute to the $\mu \to e\gamma$ branching ratio at a level which is at least ten orders of magnitude below the present limit. See [1–3] for some recent reviews.

Theoretical work on physics beyond the Standard Model concentrates on supersymmetry and grand-unification. Supersymmetry, which eventually unifies fermions and bosons, may be discovered at LHC. Grand unification, i.e. the unification of quarks and leptons, is presently constrained best by the limits on proton stability and double beta decay. Recently it was pointed out [4] that supersymmetric unification, the combination of these two very attractive ideas, may be observed in some low-energy signals. Since all sleptons are known to be massive and should mix just like quarks do, $\mu \to e\gamma$ would proceed with the help of a sparticle propagator with a branching ratio in the region $10^{-12\pm2}$, i.e. within reach of this search.

Triggered by these exciting prospects, more sensitive searches are presently being designed. Whereas $\mu - e$ conversion ranks among the two top-priority experiments for the future AGS program at the Brookhaven National Laboratory [5], the feasibility of a $\mu \to e\gamma$ search at PSI is being studied by various research groups. Both initiatives were discussed at recent workshops and the improvements over previous experiments by 2-3 orders of magnitude seem feasible.

At the moment the decay is searched for by the MEGA collaboration at LAMPF. This experiment stopped data-taking in 1995. The analysis of 16% of the data resulted in an upper limit of $4.2 \cdot 10^{-11}$ (90% C.L.) [6].

We intend to improve the sensitivity to the branching ratio for the decay $\mu \to e\gamma$ to the level of 10^{-14}. Presently, only PSI delivers the high-intensity, low-momentum, DC beams required for such an experiment. At two workshops at PSI † various designs for the detection system were discussed. Two options, both for the positron and the photon detector, were selected for further study. The two options for the positron arm are:

- An intermediate-focusing spectrometer with tracking. This spectrometer would

---

†Workshop on *a new $\mu \to e\gamma$ Experiment at PSI*, March 5–7, 1997.
Working Meeting on *A $\mu \to e\gamma$ Experiment at PSI?*, March 16–18, 1998.

have 5% momentum acceptance, 10% of 4π solid angle and 100 keV momentum resolution.

- A solenoidal spectrometer with a thin coil transparent to most photons at 50 MeV. The major advantage compared to the intermediate-focusing spectrometer is the possibility to use a thinner target extending along the beam line, thus reducing the error on $e-\gamma$ opening angle.

The two options for the photon arm are:

- A 0.6 m^3 liquid Xenon detector ("mini-Kamiokande"). By measuring the spatial distribution of the scintillation light on all faces of the tank, it will be possible to reconstruct the interaction point of the photon with a resolution of a few millimeter's.

- A more conventional scintillator array, possibly of NaI(Tl) or GSO, preceeded by a sophisticated pre-shower detector for the ultimate position and timing resolution. The pre-shower detector would be made out of Cerium doped LuAP/YAP, and read through the front face in a way similar to mini-Kamiokande.

A decision will be based on more precise estimates of the background levels and on test results with various prototypes of the photon detector. The submission of an experiment proposal to PSI would have to await such decision.

A. Tests of lepton-flavor conservation

The principle of LFC is based primarily on empirical evidence. Searches for LFC-violating decay modes of charged leptons, mesons and Z^0 have resulted in upper limits only, as summarized in Table I. Since the experimental sensitivities are mostly limited by the available beam intensities or luminosities the most stringent limits come from μ and K decays. The best limits have thus been obtained for transitions between the lighter two generations. In models, in which the couplings involving the third generation are strongly enhanced, the constraints from Z, τ and B decays start to become interesting too.

TABLE I. Branching ratios of some LFC-violating decay modes. All values are upper limits at 90% confidence, with the exception of the Z^o results, which are given at the 95% confidence level. The results are taken from Ref. [7] unless quoted explicitly.

Decay mode	Branch. Ratio	Ref.
$\mu^+ \to e^+\gamma$	$< 4.2 \times 10^{-11}$	[6]
$\to e^+e^+e^-$	$< 1.0 \times 10^{-12}$	
$\mu^- S \to e^- S$	$< 7 \times 10^{-11}$	
$\mu^- Ti \to e^- Ti$	$< 6.1 \times 10^{-13}$	[8]
$\to e^+ Ca^*$	$< 3.6 \times 10^{-11}$	
$\mu^- Pb \to e^- Pb$	$< 4.6 \times 10^{-11}$	
$\mu^+ e^- \leftrightarrow \mu^- e^+$	$< 3.5 \times 10^{-10}$	[9]
$\tau \to e\gamma$	$< 2.7 \times 10^{-6}$	
$\tau \to \mu\gamma$	$< 3.0 \times 10^{-6}$	
$\tau \to$ 3 charged leptons	$< 4 \times 10^{-6}$	
$K^+ \to \pi^+\mu e$	$< 2.1 \times 10^{-10}$	
$K^o_L \to \mu e$	$< 3.3 \times 10^{-11}$	
$B^o \to \mu e$	$< 5.9 \times 10^{-6}$	
$\to \tau e$	$< 5.3 \times 10^{-4}$	
$\to \tau\mu$	$< 8.3 \times 10^{-4}$	
$Z^0 \to e\mu$	$< 1.7 \times 10^{-6}$	
$\to e\tau$	$< 9.8 \times 10^{-6}$	
$\to \mu\tau$	$< 1.7 \times 10^{-5}$	

B. Theoretical motivation

Although the Standard Model has accomplished amazing success in describing all present experimental observations many fundamental questions in particle physics are not addressed. Numerous experimental efforts therefore focus on searches for new phenomena which would lead to a better understanding of the underlying laws of nature.

Recently the interest in LFV processes has

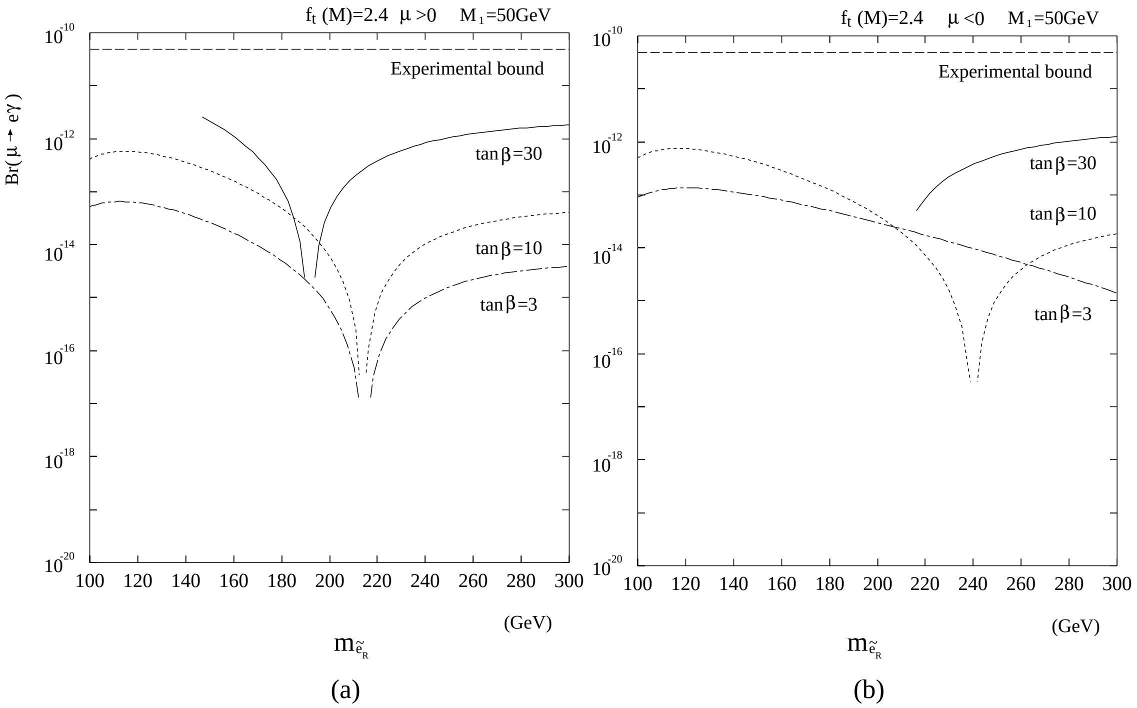

FIG. 2. Predictions of $\mu^+ \to e^+\gamma$ branching ratio in SU(5) SUSY models.

grown considerably since they appear naturally in supersymmetric (SUSY) extensions to the Standard Model, in particular in supersymmetric, grand-unified theories (SUSY-GUT). Although the soft-breaking scalar mass matrices (such as the slepton matrix) are assumed diagonal and universal at the Plank scale, radiative corrections in the renormalization group evolution from the GUT to the weak energy scale unavoidably lead to slepton mixing [11]. As a result $\mu^+ \to e^+\gamma$ occurs through loop diagrams as shown in Fig. 1. Recently, Barbieri and Hall [4] found that the mixing is even quite large owing to the large top-quark Yukawa coupling and their predicted branching ratio is within reach of near-future experiments. In SU(5) SUSY-GUT models the width for $\mu^+ \to e^+\gamma$ can be approximated by [4]:

$$\Gamma(\mu \to e\gamma) \approx \frac{\alpha}{4}\Big|\frac{\alpha M_Z}{24\pi \cos^2\theta_W}\frac{\Delta m^2_{21}}{m^2_{\tilde{\mu}}}\Big|^2 \frac{m^5_\mu}{m^4_{\tilde{\mu}}}$$
$$\Delta m^2_{21} = -V^*_{32}V_{31}I(y_t)\ ,$$

where $I(y_t)$ is a function of the top-quark Yukawa coupling y_t, V_{ij} is the Cabibbo-Kobayashi-Maskawa quark mixing matrix at some GUT energy scale, and m_μ and $m_{\tilde{\mu}}$ are muon and smuon masses, respectively. The branching ratio of $\mu^+ \to e^+\gamma$ predicted in SUSY SU(5) models [12] is shown in Figure 2. The prediction varies from 10^{-15} to 10^{-13} for

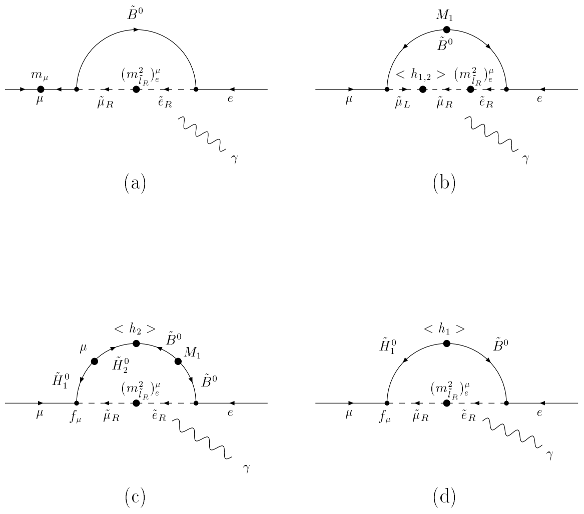

FIG. 1. Diagrams of $\mu^+ \to e^+\gamma$ in SU(5) SUSY models.

the singlet smuon mass of $m_{\tilde{\mu}_R}$ of 100 to 300 GeV. SO(10) models give even values which are enhanced by a factor $(m_\tau/m_\mu)^2$ [4] resulting from loop diagrams which contribute in proportion to the lepton mass. In all these models, $\mu^- - e^-$ conversion in nuclei has a branching ratio which is typically 200 times lower.

Non-vanishing neutrino masses and mixing, as suggested by the atmospheric neutrino anomaly, might invoke additional LFV contributions. In an SU(5) SUSY-GUT model [13] with a heavy right-handed Majorana neutrino of $10^{14} - 10^{15}$ GeV and mixing of $\sin^2(2\theta_{\nu_\mu\nu_\tau}) \sim 1$ (as suggested by Super Kamiokande) LFV is enhanced by a factor $(m_\tau/m_\mu)^2$. The predicted branching ratios are shown in Fig. 3 for m_{ν_τ}=0.07 eV assuming

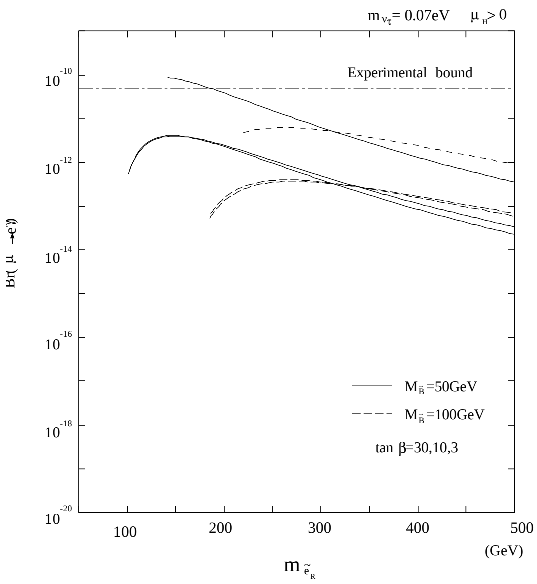

FIG. 3. Predictions for the $\mu^+ \to e^+\gamma$ branching ratio in SU(5) SUSY models with right-handed Majorana neutrino as a function of m_{e_R} assuming the Yukawa coupling constant of ν_τ is equal to that of the top quark.

the ν_τ Yukawa coupling equal to the top-quark Yukawa coupling. Non-unified SUSY models with a right-handed massive Majorana neutrino predict a similar $\mu^+ \to e^+\gamma$ branching ratio [14].

II. GENERAL CONSIDERATIONS

A. Sensitivity

The signature for a $\mu^+ \to e^+\gamma$ decay at rest is an $e^+\gamma$ pair, coincident in time, moving back-to-back with momenta equal to half the muon mass (52.8 MeV/c). The single event sensitivity is given by

$$S(\mu^+ \to e^+\gamma) = \frac{1}{N_\mu \cdot t \cdot (\Omega/4\pi)} \times \frac{1}{\varepsilon_e \cdot \varepsilon_\gamma \cdot \varepsilon_{cut} \cdot f_S}\ , \qquad (1)$$

where N_μ is the muon stop rate, t is the measuring time, Ω is the detector solid angle, ε_e and ε_γ are the positron and photon detection efficiencies, ε_{cut} is the efficiency of the selection cuts, and f_S is a correction factor in the case of polarized muons (f_S=1 for unpolarized muons). Take, for example, $N_\mu = 3 \times 10^8 s^{-1}$, $t = 10^7$ s, $\Omega/4\pi = 0.1$, $\varepsilon_e = 0.9$, $\varepsilon_\gamma = 0.8$, $\varepsilon_{cut} = 0.6$, $f_S = 1$, then $S = 0.8 \times 10^{-14}$, corresponding to a 90 % C.L. upper limit of 2×10^{-14} if no event candidates are found.

B. Backgrounds

In the following sections, the normalized e^+ and photon energies are used, defined as $x \equiv 2E_e/m_\mu c^2$ and $y \equiv 2E_\gamma/m_\mu c^2$. Furthermore, $z \equiv \pi - \theta_{e\gamma}$ and δA (ΔA) is defined as half width (full width) of the cut on the observable A.

1. prompt background

Prompt (physics) background originates from radiative muon decay $\mu^+ \to e^+\nu\overline{\nu}\gamma$. The differential decay width, for $x \sim 1$ and $y \sim 1$, is given by [16]

$$dB_{rad}/d\cos\theta_e = \alpha/16\pi \times [J_1(1 - P_\mu \cos\theta_e) + J_2(1 + P_\mu \cos\theta_e)\ ]\ , \quad (2)$$

where θ_e is the e^+ emission angle relative to the muon spin direction. Without constraint on the opening angle $\theta_{e\gamma}$ (CASE1) J_1 and J_2 are given by:

$$J_1 = (\delta x)^4(\delta y)^2 \quad \text{and} \\ J_2 = (8/3)(\delta x)^3(\delta y)^3 \,. \tag{3}$$

A constraint on δz affects dB_{rad} only if $\delta z < 2\sqrt{\delta x \delta y}$ (CASE2), in which case:

$$\begin{aligned} J_1 &= (8/3)(\delta x)^3(\delta y)(\delta z/2)^2 - 2(\delta x)^2(\delta z/2)^4 \\ &\quad +(1/3)(1/\delta y)^2(\delta z/2)^8 \quad \text{and} \\ J_2 &= 8(\delta x)^2(\delta y)^2(\delta z/2)^2 - 8(\delta x)(\delta y)(\delta z/2)^4 \\ &\quad +(8/3)(\delta z/2)^6. \end{aligned} \tag{4}$$

For unpolarized muons ($P_\mu = 0$), integration of Eq.(2) over $\cos\theta_e$ gives:

$$B_{rad} = \frac{\alpha}{8\pi}[J_1 + J_2]. \tag{5}$$

Figure 4 shows B_{rad} as a function of the cut values δx and δy for CASE1. One sees, for instance, that Δx=2(δx)=0.01 and Δy=2(δy)=0.05 lead to $B_{rad} = 2 \times 10^{-15}$, which is one order magnitude below the projected sensitivity.

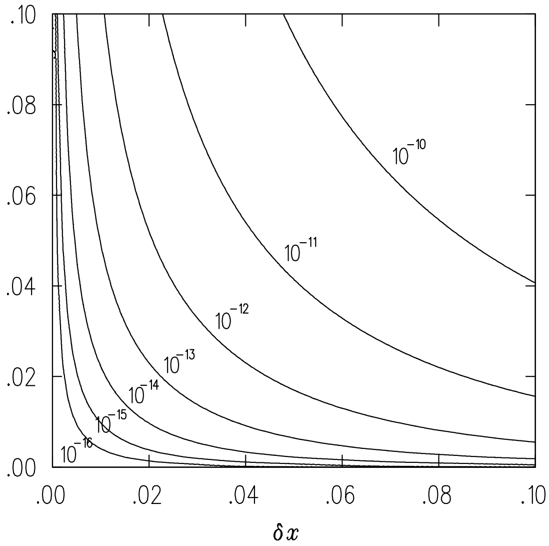

FIG. 4. Prompt background contribution from $\mu^+ \to e^+\nu\overline{\nu}\gamma$ as a function of δx and δy for CASE1.

2. accidental background

Accidental $e^+\gamma$ coincidences involve an e^+ from normal muon decay, $\mu^+ \to e^+\nu\overline{\nu}$, and a high energy photon which may originate in the decay $\mu^+ \to e^+\nu\overline{\nu}\gamma$ or from an e^+ through external bremsstrahlung or annihilation in flight. The number of accidental coincidences is given by:

$$\begin{aligned} N_{acc} = \quad & N_\mu \cdot f_e^0 \cdot \Omega/4\pi \cdot \varepsilon_e \\ & \times N_\mu \cdot f_\gamma^0 \cdot \Omega/4\pi \cdot \varepsilon_\gamma \\ & \times \delta\omega/\Omega \cdot 2\delta t \cdot t \cdot f_{P_\mu} \,, \end{aligned} \tag{6}$$

where f_e^0 and f_γ^0 are the e^+ and γ yields per stopped muon, respectively, and f_{P_μ} is a correction factor for polarized muons [17]. P_μ=0 is considered from now on. The solid angle cut $\delta\omega$ depends on the angular cut as:

$$\frac{\delta\omega}{4\pi} = \frac{\pi(\delta z)^2}{4\pi} = (\frac{\delta z}{2})^2 \tag{7}$$

The effective branching ratio for accidental background is obtained from:

$$B_{acc} = \frac{N_{acc}}{N_\mu \cdot t \cdot (\Omega/4\pi) \cdot \varepsilon_e \cdot \varepsilon_\gamma} \,. \tag{8}$$

For unpolarized muons, B_{acc} becomes

$$B_{acc} = N_\mu \cdot f_e^0 \cdot f_\gamma^0 \cdot \frac{\delta\omega}{4\pi} \cdot 2\delta t \cdot f_{P_\mu} \tag{9}$$

The e^+ yield f_e^0 is obtained by integrating the Michel spectrum, $2x^2(3-2x)$, above $1-\delta x$:

$$f_e^0 = 2(\delta x) \tag{10}$$

In estimating f_γ^0 first the radiative muon decay ($\mu^+ \to e^+\nu\overline{\nu}\gamma$) is considered [17]:

$$f_\gamma^0 = \frac{\alpha}{2\pi}(\delta y)^2\Big[\ln(\delta y) + 7.33\Big] \tag{11}$$

The result is shown in Fig.5 [18]. The other sources of high-energy photons are external bremsstrahlung and annihilation in flight of e^+s from normal muon decay. Since the muon

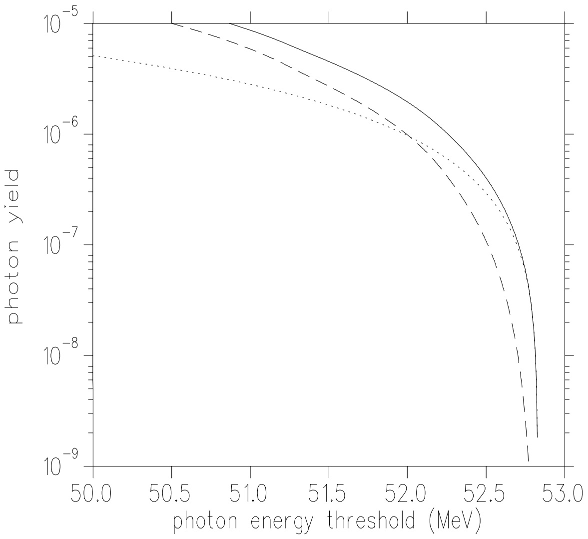

FIG. 5. Photon yields v.s. energy threshold: dotted, from annihilation in flight in a 50 mg target; dashed, from radiative muon decay; solid, sum of the two.

stopping target may be very thin external bremsstrahlung of decay positrons in the target is small compared to the internal process. By taking care that positrons can not reach any material in direct sight of the photon detector this process can be ignored altogether.

The contribution from annihilation in flight for a 50 mg/cm^2 target, is shown in Fig.5 as well. In this case annihilation in flight dominates for photon energies above 52 MeV.

From the above, the effective branching ratio of accidental background is given by:

$$B_{acc} = N_\mu \cdot 2\delta x \cdot \frac{\alpha}{2\pi}(\delta y)^2(\ln(\delta y) + 7.33) \times (\delta z/2)^2 \cdot 2\delta t \tag{12}$$

Table II lists values of B_{acc} for different sets of cut values.

TABLE II. Accidental Background Contributions for typical examples of resolutions.

case	Δx	Δy	$\Delta\theta_{e\gamma}$	Δt	B_{acc}
	%	%	rad	ns	
1	1	2	0.01	0.3	2×10^{-15}
2	0.2	5	0.02	0.1	2×10^{-15}

III. ΠE5 SURFACE MUON BEAM

The πE5 channel extracts low-energy π and μ beams from the thick production target at an angle of 175^o with respect to the primary proton beam. A description of this beam line can be found in Ref. [19]. The main characteristics of this beam line are listed in Table III.

TABLE III. Main properties of πE5.

solid angle acceptance	150 msr
momentum range	20–120 MeV/c
length	10.4 m
momentum band (FWHM)	10%
momentum resolution (FWHM)	2%
horizontal emittance	15.3 cm.rad
vertical emittance	3.6 cm.rad
spot size	2×2 cm^2

FIG. 6. The experimental area πE5. The beam can be directed to the areas piE51 or piE52 (see text for details).

Figure 6 shows the present layout of the experimental areas. There are two modes of operation, "U" and "Z", feeding the areas πE51 and πE52, respectively. It is likely that only the πE52 area is large enough to accommodate the $\mu \to e\gamma$ experiment. Also from the

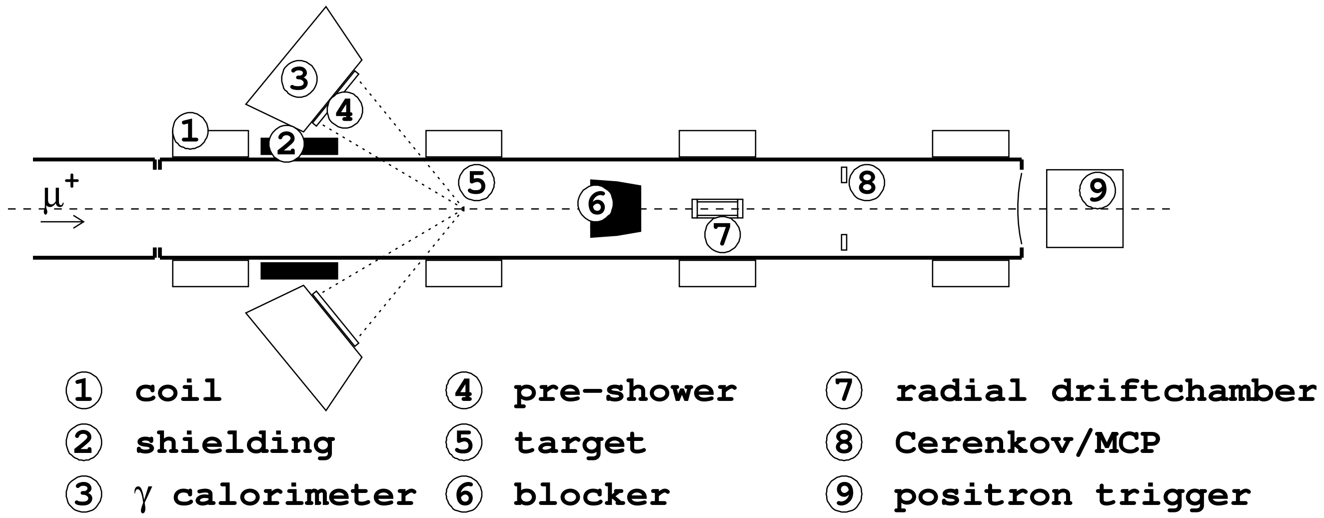

FIG. 7. Intermediate-image spectrometer

point of view of beam optics the "Z" mode is preferred.

Until the year 2000 the area will be occupied by the SINDRUM II spectrometer. In this experiment the beam is extracted with the help of a solenoid with a diameter of 40 cm. This large aperture is necessary to collect the beam which has a focus inside the last bending magnet. For the $\mu \to e\gamma$ experiment the channel would be tuned to $\approx 28MeV/c$ to collect so-called surface muons, i.e. muons originating in the decays of pions which stopped close to the surface of the production target.

Since such beam has not been studied yet there is some uncertainty about the intensity, which is expected in the region 4–8$\times 10^8 \mu^+$/s at a proton current of 1.5 mA. In practice the rate will be reduced in an attempt to minimize the target dimensions which affect the positron momentum and angular resolutions. Given these uncertainties we intend to perform some beam studies during the second half of 1998.

Serious problems may be caused by the positrons in the beam which are typically ten times more abundant than the muons. For this reason a particle DC separator is required or at least very useful, depending on the experimental layout. Such device would lead to a beam loss of typically 30%.

Another concern are the fluxes of high-energy and thermal neutrons, which might raise the background level in the photon detector. We intend to study the neutron fluxes and the possibilities to reduce this background source by local shielding.

IV. OPTIONS FOR THE DETECTION SYSTEM

Various options are under active study, both for the positron spectrometer and for the photon detector. Two possibilities will be discussed here (see Fig. 7 and Fig. 8). As positron spectrometer we consider:

- A two-stage intermediate image spectrometer with tracking detectors in the second stage.

- A solenoidal spectrometer with a thin coil, which allows the use of a photon detector outside the coil. Two different options for the tracking chambers will be described.

As photon detector we consider:

- A liquid Xenon detector, equipped with photo-detectors on all sides for optimal position, timing and energy resolutions.

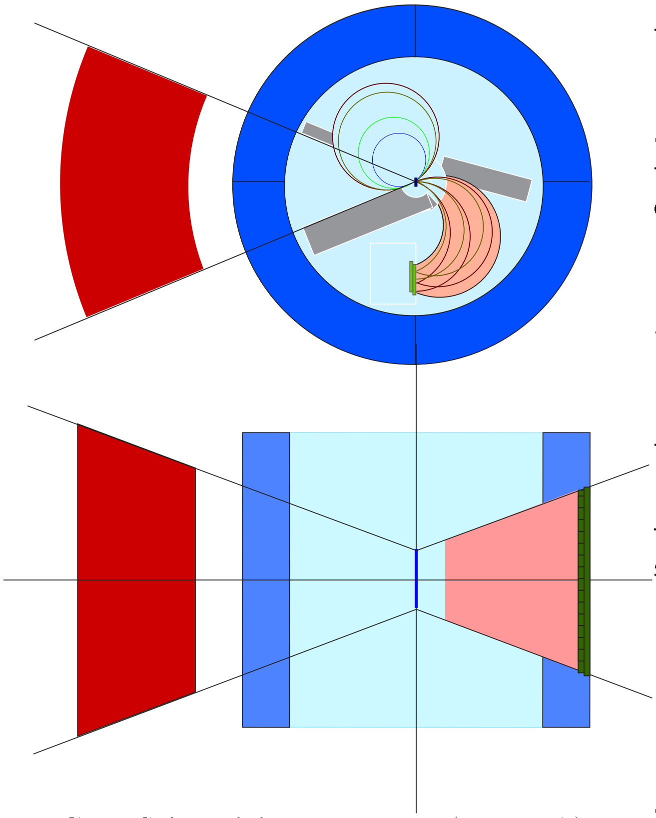

FIG. 8. Solenoidal spectrometer (Design A). Top: axial view of a setup with solenoidal e^+ spectrometer and photon detector on the left. Multiple e^+ crossings are suppressed with the help of shielding walls.
Bottom: side view of the setup.

- A hybrid detector, consisting of a segmented photon calorimeter preceeded by a pre-shower detector for optimal position and timing resolutions.

A. Positron spectrometer

1. intermediate focusing spectrometer

Intermediate image spectrometers were developed some 50 years ago for β-ray spectrometry. Momentum resolution was obtained by momentum selection, using variable field strengths to scan a certain momentum interval. Momentum resolution was dependent on focus quality, which gave certain limitations to source size and opening angle acceptance. With the help of tracking detectors many of these limitations disappear and dramatic improvements in resolution and/or acceptance can be achieved. The tracking detectors can be protected against the vast number of positrons emitted at lower momenta. By positioning the tracking detectors at the periodic focus locations their influence on the momentum determination can be minimized. The focusing also leads to an enormous simplification of the trigger for data readout and, last but not least, makes it much easier to obtain a superb time signal.

The simplest φ-symmetric spectrometer field is the constant field generated by a solenoid. In such a field particles emitted at larger angle with respect to the symmetry axis return to the axis at shorter distance and at best one may observe a sort of ring focus. A reduction of the field strength towards larger radii will lengthen the focusing distance for larger angles and may thus improve the focusing properties. The simplest configuration which generates the required field shape is a series of coils. In the following we describe the focusing properties of a system of three identical coils, with inner radius 20 cm, outer radius 30 cm and length 40 cm, placed at a distance of 60 cm from each other. The currents are chosen such that the field strength in the center of each coils is 1.877 T, optimized for particles of 50 MeV/c, emitted from a point source at $\theta = 40^o$. Figure 9 shows the resulting trajectories. A large angular band is transmitted and the particles are nicely focused at end.

Transmission

Figure 10 shows distributions of the distance to the axis as a function of momentum, emission angle and source size. The point source distributions show almost perfect focusing over an angular range of $30^o - 50^o$, corresponding to a solid angle of 11%. The momentum dispersion is practically zero and the optimum momentum, in terms of focal quality, shifts to 48 MeV/c when increasing the source from pointlike to a ring with 2 cm radius. For

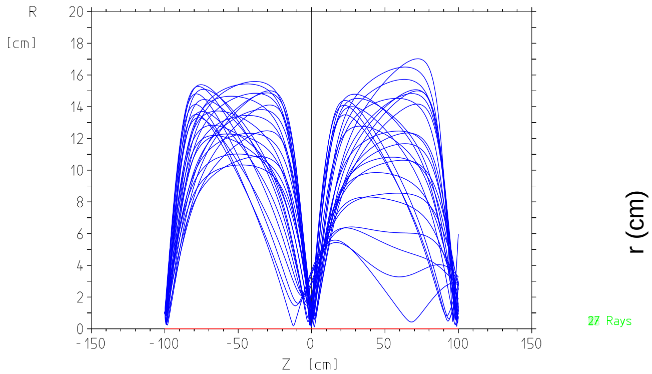

FIG. 9. Trajectories (distance to the symmetry axis v.s. z) for a ring source with 1 cm radius at 50 MeV/c and θ in the range $30^o - 50^o$.

such extended source the field would have to be raised by 10%.

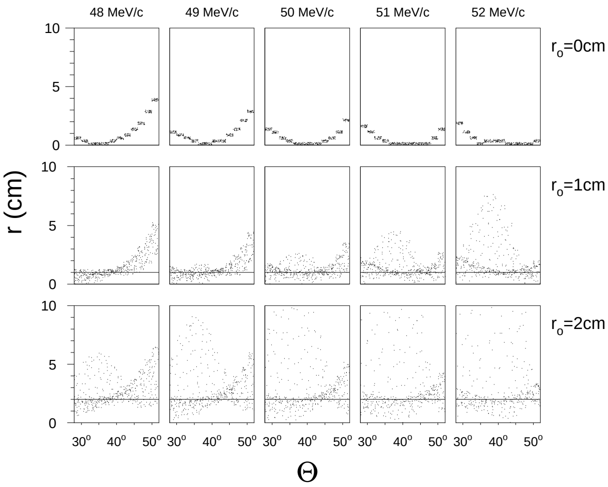

FIG. 10. Distributions of r, the distance to the symmetry axis, after one spectrometer stage as a function of θ for various values of the particle momentum and ring-source radius r_0.

Momentum dispersion

The symmetry of the field with respect to the plane halfway between the coils leads to a second, intermediate, focus as is demonstrated in Fig. 11. Contrary to the "real" focus, this intermediate focus shows a very large momentum dispersion: a 10% change in momentum leads to a 50% change in radial coordinate. As has been known for intermediate image spec-

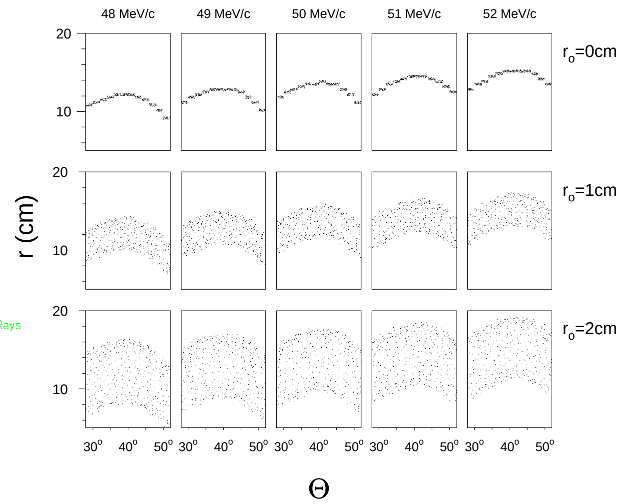

FIG. 11. Distributions of r, the distance to the symmetry axis, halfway one spectrometer stage as a function of θ for various values of the particle momentum and ring-source radius r_0.

trometers there is a large broadening due to the source size. By measuring the trajectory in both focal planes the source contribution can be corrected, as will be demonstrated below.

Extended-source effect

Assume three position detectors, one in the focal plane and two close to the intermediate plane, used to determine the coordinates r_i, φ_i, i=1,2,3, respectively. Polynomials in these coordinates were found for momentum and angle. The expressions are good to within 100 keV and 1^o (FWHM). The contribution to the momentum resolution from the finite detector resolution has been determined by error propagation. Figure 12 shows the resulting momentum resolution as a function of source size and θ. A position resolution of ± 0.1 mm is sufficient to reach a momentum resolution below ± 50 keV. It is remarkable that the requirements on the resolution of the focal-plane detector are less stringent than for the detectors around the intermediate plane.

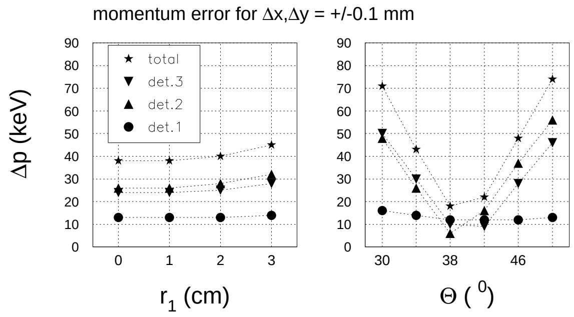

FIG. 12. Momentum error, caused by finite position resolution, as a function of the distance to the origin and the emission angle. The strong θ dependence is a direct consequence of the corresponding focal resolution, observed in Fig. 11.

Tracking detectors

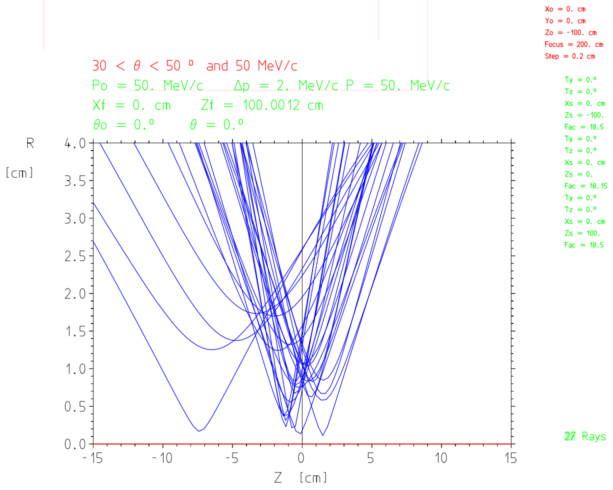

FIG. 13. Close-up of the trajectories shown in Fig. 9 in the region of the first focus.

Figure 13 shows the trajectories in the region of the first focus for a source with 1 cm radius. Figure 14 shows the same trajectories in the $x - y$ view. All trajectories approach the symmetry axis to within 2 cm and most of them cross the planes at $z = \pm 7.5$ cm at r >3.5 cm. For this reason the tracking detector may be a radial drift chamber with a length of about 15 cm, an inner radius of 2.5 cm and an outer radius of 3.5 cm.

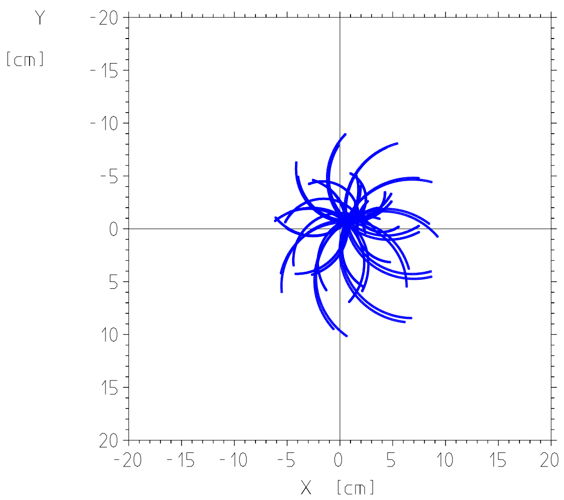

FIG. 14. Trajectories as in Fig. 13, but in the $x - y$ projection.

Further study includes the effects of return iron, required to reduce the stray field at the location of the photon calorimeter, and the addition of trim coils to improve the performance. At the same time tracking detectors will have to be defined in more detail to estimate their influence on momentum and angular resolution.

2. solenoid

General Description

This option aims at the best resolution for the opening angle between the positron and the photon. This is achieved by using a very thin extended target, slanted at a small angle relative to the beam direction. The solenoid field appears to be the best choice in combination with such an extended target.

A target of thickness below 2×10^{-4} radiation length, possibly less than 200 μm polyethylene, is placed in the center of the solenoid at an angle of about 6^o to the beam axis. This target causes an uncertainty of 1.7 mrad in projected planes of the positron emission angle.

A photon detector is placed outside the solenoid magnet while a positron tracking system is installed inside. The solenoid field sweeps charged particles away from the photon calorimeter with a minimal stray field at the location of the phototubes of the photon calorimeter. Thin wall super-conducting solenoid magnets are commonly used in particle physics experiments these days.

After the successful experience with a superconducting, thin-wall (0.2 radiation lengths) solenoid magnet (Fig.15), a new

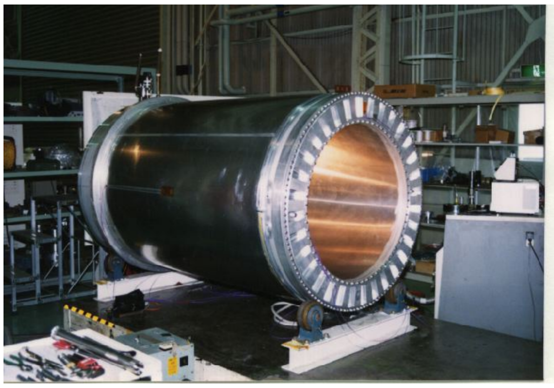

FIG. 15. BESS thin wall super-conducting solenoid magnet.

magnet with the total thickness of 0.1 radiation lengths, which leads to a loss of only 5% of 50 MeV photons, is currently under design. The operating magnetic field is assumed to be 1 Tesla, which confines 52.8 MeV positrons within the inner diameter of the solenoid (≈75 cm).

Good angular and momentum resolutions are obtained by minimizing the material along the positron trajectories. A gas chamber, one kind or another, appears to be the only tracking detector that fulfills the requirements. The chamber gas must be selected from the view point of minimal material and high rate capability. Current choice is 90% helium and 10% ethane or 50% helium and 50% ethane.

In a solenoid-field spectrometer (as in MEGA), curling tracks of the positrons emitted at $\approx 90^o$ might cause multiple hits in the chambers. Two different solutions are currently under discussion. In the first design (Design A, see Fig. 8), positrons are stopped after their 180^o turns in a heavy metal shielding. In the second design (Design B, see Fig.16) the tracking wires are kept away from the target so that they see only particles with transverse momentum above 35 MeV/c. The central part of the sense wires is made insensitive by special coating. In addition, a slight gradient in the magnetic field will sweep all positrons out of the active area quickly.

Design A

The configuration is shown in Fig.8. The active volume of the wire chambers starts at 10 cm from the target and reaches up to $\sim 90^o$ to the horizontal plane. The chamber covers those 52.8 MeV positrons emitted at -22.5^o to $+22.5^o$ and pitch angle of tracks from -23.6^o to $+23.6^o$ Behind the tracking chambers, two layers of scintillation counter hodoscopes define the acceptance (5% at 52.8 MeV) and are used for triggering and time measurement.

Momentum resolution of the spectrometer is limited by multiple scattering in the chamber gas to be about 0.2 % as long as the position resolution of the chamber does not exceed 100–300 μm. More important than the momentum determination are the measurements of the emission angle of positrons and its extrapolated position at the target. The resolutions of these quantities are also primarily determined by the multiple scattering due to the chamber gas. For the combination of a polyethylene target of about 0.2 mm thickness and He/C_2H_6 (90%/10%) as chamber gas, these resolutions could be about 6 mrad and 1.5 mm, respectively.

The first layer of the tracking chambers suffers most from high counting rates. The major source of particles firing the wires are positrons from the Michel decay of muons in the target. For $3 \times 10^8 \mu^+$ decays per second, the first chamber, which covers about 9% of the full solid angle, would have a total count rate of 1.4×10^7 e^+/s, corresponding to 8×10^2 e^+/s/mm^2 and 1.4×10^5 e^+/s/wire assuming about 100 anode wires. The corresponding rate in the last detector plane is 4.5×10^6 e^+/s, or about 100 e^+/s/mm^2.

Design B

In this design, positron tracks are measured

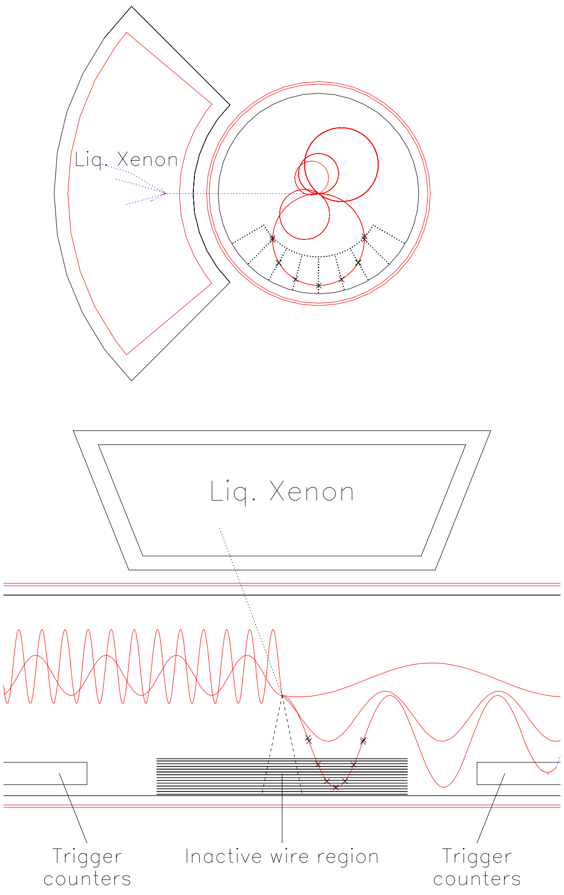

FIG. 16. Solenoidal spectrometer (Design B). Shown is the event of a $\mu \to e\gamma$ decay with four accidental Michel tracks superimposed.

with a cylindrical wire plane at a radius of about 23 cm and a number of planes aligned radially at 15^o intervals in azimuthal angle. They could be either MWPCs or drift chambers. The sense wires are made inactive at the central region ($|\cos\theta| < 0.2$) by special coating so that the curling tracks should not cause too much problems. 52.8 MeV positrons emitted from the target with $0.15 < |\cos\theta| < 0.65$ and $-30^o < \phi < 30^o$ produce at least six hits in the tracking chambers. The resulting acceptance is about 8 %.

In the case of drift chambers each plane may consist of a few staggered layers. By selecting aligned hits in adjacent wire cells off-timing hits ($\Delta t > 15$ ns) are effectively removed. For a μ^+ stop rate of 3×10^8 /s, a typical $\mu^+ \to e^+\gamma$ event would look like in Fig. 16 assuming an effective time-gate of 15 ns width.

Trigger scintillation counters are placed at $|z| > 70$ cm and $r > 24$ cm, far enough to protect the photon detector from the photons produced. The timing resolution should be about 50 ps.

The offline track reconstruction would start from the outside, where the rate is lowest. Assuming a space resolution of 150 μm, which corresponds to 4 ns drift time in He/C_2H_6 (50/50), the accidental hits from Michel positrons should pose no problems even at the innermost layer. A realistic Monte Carlo simulation is currently under way.

The momentum resolution is estimated to be 0.2 % (σ). The angular resolution is determined by multiple scattering to be around 6 mrad. The resolution of the position extrapolated to the target will be about 1.5 mm.

B. Gamma detector

1. liquid xenon scintillation detector

With its high light yield and short decay time (see Table IV), liquid Xenon scintillator potentially achieves the energy and time resolution required for this experiment.

In the “mini-Kamiokande” scheme adopted here (see Fig. 17), a single tank (0.5–0.7 m^3) filled with liquid Xenon is viewed from all sides by arrays of photo-multiplier tubes (PMTs). PMTs that are sensitive to the 175nm scintillation light and work at liquid Xe temperature have been developed in collaboration with Hamamatsu Photonics [22]. They were immersed in the liquid Xe and the scintillation light from ^{241}Am α particles has been measured (Fig. 18).

TABLE IV. Properties of Liquid Xenon

Density	3.00 g/cm^3
Boiling and melting points	165 K, 161 K
Radiation length	2.77 cm
Scintillation wave length	175 nm
Energy per scintillation photon	24 eV [20]
Decay time	45 ns (75%) [21]
	22 ns, 4.2 ns
Scintillation absorption length	> 100 cm
Attenuation length (through Rayleigh scattering)	30 cm

Detailed Monte Carlo simulations are performed to investigate the expected position and energy resolutions. A 50 MeV γ ray entering the liquid Xenon loses most of its energy near the entry point, typically within 2–10 cm from the surface, resulting in a distribution of the PMT outputs as shown in Fig. 19(a). In the simulation the PMTs are spaced at 6 cm. According to the simulation the γ position, using the weighted mean of this distribution, can be determined to a precision of $\sigma \approx 1.7$ mm (Fig. 19(b)). The depth of the γ interaction point can be determined with a precision of $\sigma \approx 7$ mm.

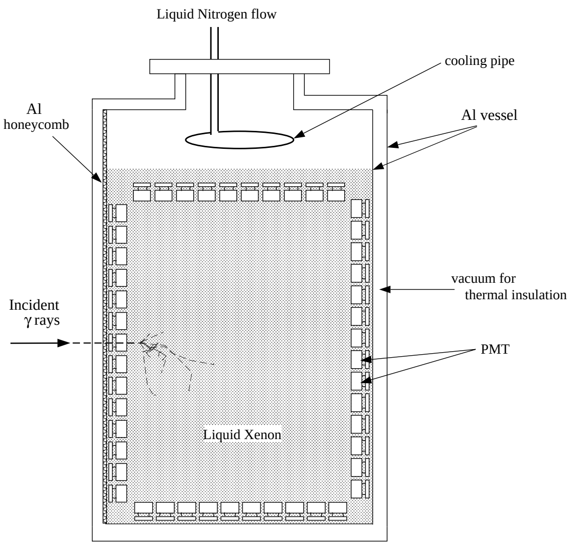

FIG. 17. Schematic view of the "mini-Kamiokande" calorimeter. A simulated 52.8 MeV γ shower is superimposed.

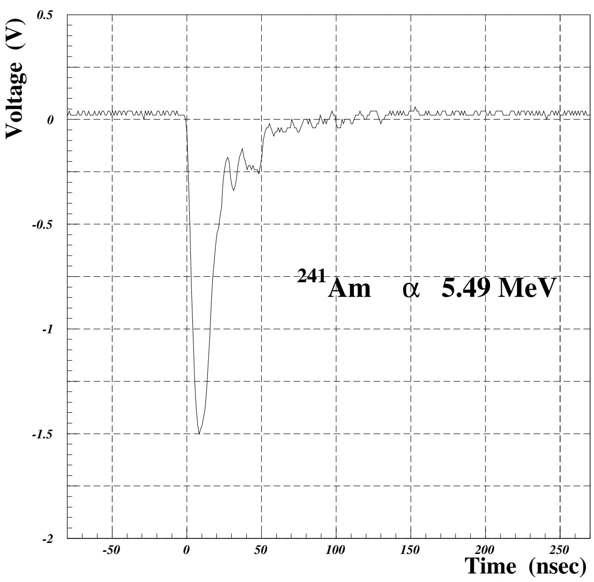

FIG. 18. A liquid Xe signal observed for a 5.49 MeV α particle.

The complete coverage with PMTs allows to correct the position-dependent light collection and timing; an energy resolution of a few % and a timing resolution around 200 ps may be expected. Low-energy γ rays produced in the shower tend to travel far and may escape the calorimeter. Figure 20 shows the distribution of the energy fraction deposited within a certain radius in liquid Xe by 52.8 MeV γ rays. For a precise energy measurement the detector has to be extended laterally by 20 cm. It also

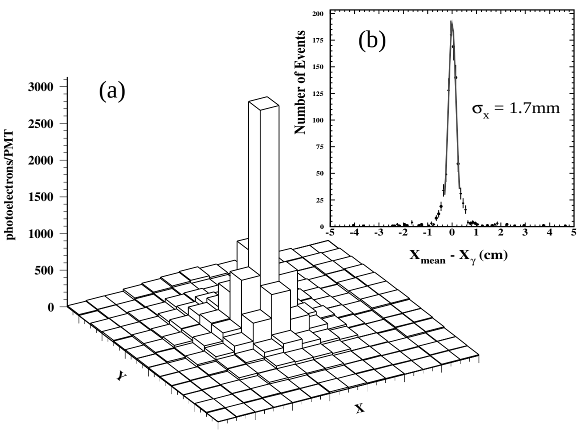

FIG. 19. (a) Spatial distribution of light observed for the event in Fig. 17; (b) Distribution of the position error using weighted-mean.

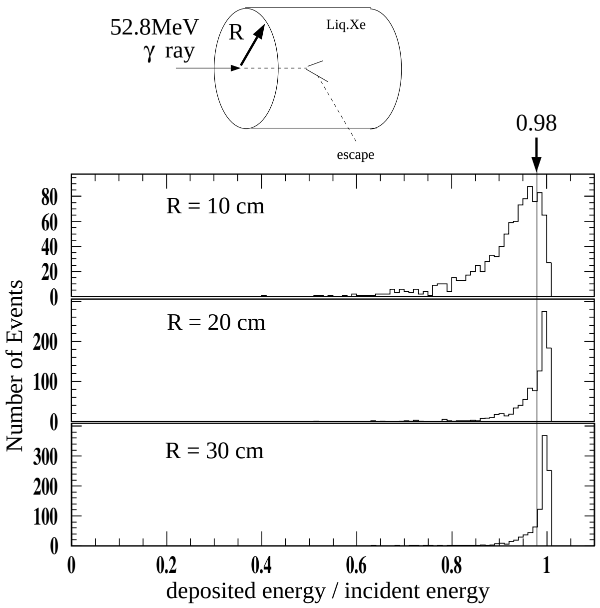

FIG. 20. Fraction of energy deposited in liquid Xe within a given radius R.

implies that segmentation of the calorimeter is useless.

Pile-up of γ rays could increase the accidental background. Fig. 21 shows a simulation of

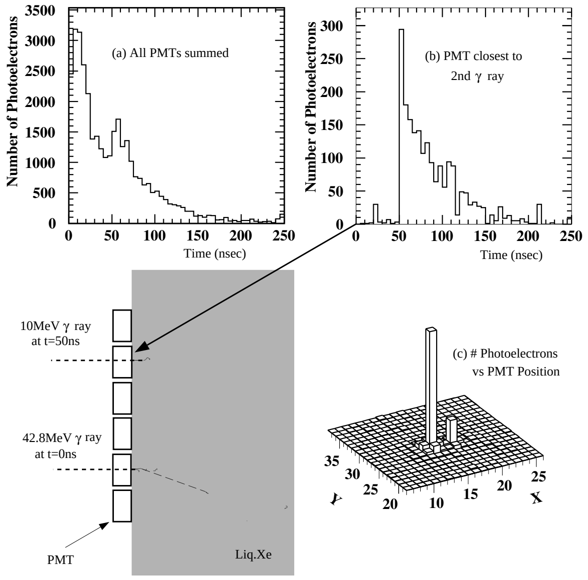

FIG. 21. A simulated event in which a 43 MeV photon is followed after 50 ns by a 10 MeV photon. Top left: wave form (all PMTs summed); top right: wave form of the PMT closest to the 10 MeV γ; bottom right: spatial distribution of the scintillation light.

a potential pile-up event. Wave-form digitizers will be used to help identify the event. For example, two γ rays, each with an energy greater than 5 MeV, can be reconstructed if their time difference is more than 10 ns. A MC study, taking into account inner Bremsstrahlung, annihilation in flight in the target, and positron interactions in the surrounding materials, indicates that pile-up background is under control.

A small prototype detector with 32 PMTs is under construction (Fig. 22) to be used to study the detection principle with γ sources.

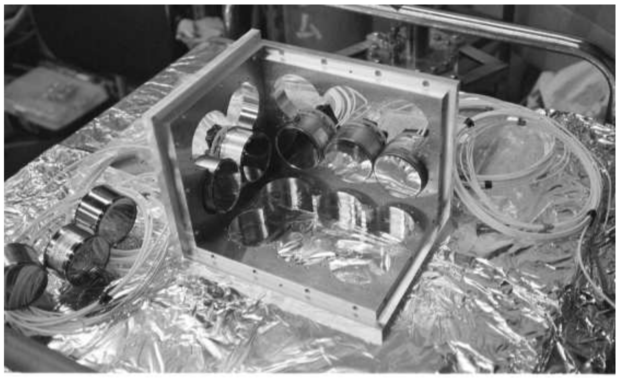

FIG. 22. The prototype detector with 32 PMTs being assembled.

2. Crystal calorimeter with pre-shower

In this scheme the photon detector consists of an electromagnetic calorimeter of conventional geometry, preceded by a pre-shower detector. The latter not only determines the photon conversion point with a precision of a few millimeter's, but allows for extremely high timing resolution, which is important, since the potential background in this experiment is dominated by accidental coincidences.

The pre-shower detector would have an area of about 0.5 m^2 and a thickness of 2 cm and consist of about 50 single crystals. The readout would be configured as in an Anger camera with the help of some 450 small photo-detectors (photomultipliers or photodiodes) mounted on the front face of the detector. Figure 23 illustrates the principle. As

TABLE V. Properties of scintillating crystals.

	Ce concentration	light yield	fall time	density	peak wave length	energy resolution[a]	time resolution[b]	mass attenuation[c]	refractive index
YAP	0.5	18	25	5.3	365	5.7	0.16	2.63	1.94
LuAP	0.10	11	16	8.4	365	9.3	0.16	1.05	1.94
LSO	0.22	27	47	7.4	420	10	0.16	1.05	1.82
GSO	1.0	8	41	6.7	420	8.5	0.70	1.38	1.85
BGO	–	9	300	7.1	490	10	1.0	1.11	2.15
NaI(Tl)	–	40	230	3.7	415	6.5	0.35	3.05	1.85
	%	ph/keV	ns	g/cm^3	nm	%	ns	cm	

[a] at 660 keV [b] at 1 MeV [c] at 511 keV

scintillating medium we consider one of a small number of isostructural rare-earth orthoaluminates (perovskites) whose most prominent members are $YAlO_3$ (YAP) and $LuAlO_3$ (LuAP), but also $YbAlO_3$ appears to be a very promising candidate. When activated with Ce^{3+}, these crystals have very similar spectroscopic and scintillation properties. Compared to a commonly used scintillator, such as NaI(Tl), the light yield is up to 50 percent and the decay time constant is shorter by an order of magnitude. Table V lists the relevant properties for a number of scintillating crystals. One of the most important parameters is the mass attenuation length which is, thanks to the higher atomic number and density, 2.5 times shorter for LuAP and YbAP, than for YAP and NaI(Tl). There are no real alternative scintillating materials for this detector. BGO is the only crystal with a similar mass attenuation, but suffers from poor energy and timing resolution.

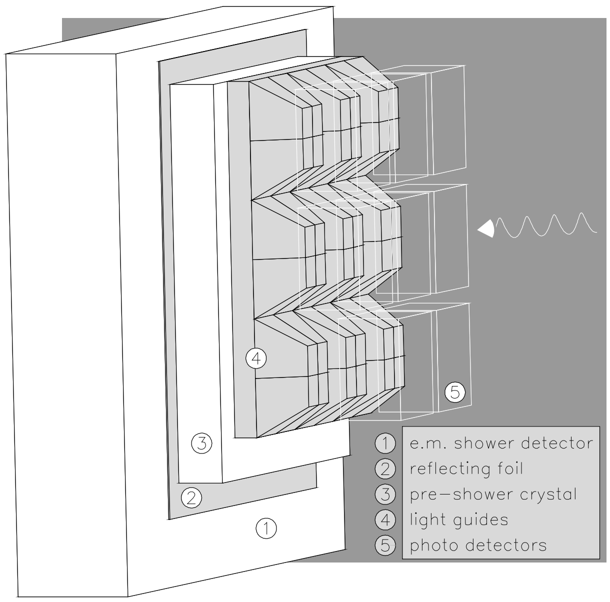

FIG. 23. Schematics of photon detector

This very high performance has been obtained despite deficiencies in the Cerium concentration and optical transparency and it is commonly believed that large improvements should still be possible. Whereas it has not yet been possible to grow large (in excess of 1 cm^3) crystals of LuAP:Ce, 100 cm^3 crystals of YAP:Ce are produced in significant quantities. It is also known that the Ce content in present crystals is well below the optimal value from the point of view of light yield. A second problem is the absorptive loss of scintillation light. The source of the absorption is not clear, but is expected to be caused by unknown impurities in the crystal.

At present it is possible to produce mixed crystals of YAP and LuAP, which fulfill all our requirements with respect to size, homogeneity, light output and photon efficiency. The reason for this lucky circumstance are their very similar excitation and absorption spectra. Still we believe that we should use the time remaining until we would start the production of the required crystals to improve the crystal quality as much as possible, in particular into the direction of:

- higher Ce concentration
- reduced parasitic absorption
- higher LuAP fraction
- larger crystal sizes

As an alternative we consider $YbAlO_3$:Ce, a crystal not yet documented in the literature, which we have started to produce just recently. At present we are investigating the detection properties of this crystal which is cheaper and easier to produce than $LuAlO_3$:Ce.

For the electromagnetic calorimeter we consider good old NaI(Tl) or GSO, i.e. another new crystal type. GSO has as main advantages over NaI(Tl) a much higher density (6.7 g/cm^2 compared to 3.7 g/cm^2) and shorter decay time (41 ns compared to 230 ns) at the cost of a fourfold reduction in light yield. This crystal can be produced in the required quantities. Alternatively we might choose for YAP or CsI(Na), an extremely bright crystal which became interesting after we succeeded to reduce the decay time from $\approx 1\mu$s to ≈ 400 ns.

V. TIME-TABLE, COSTS AND MANPOWER

time-table

A decision about the detection system will have to await further simulations and R&D, which may take one year at least. The submission of a proposal could thus take place by the end of 1999 at the earliest. Detector construction would take another three years at least, such that data-taking could take place in the years 2003-2005.

costs

Reliable cost estimates can not be given until the detection system is better defined and tenders have been put in. Rough guesses indicate that the experiment will not cost more than 10M CHF. A high transmission beam extraction system including DC separator costs about 0.5M CHF. The magnetic spectrometer may cost around 2M CHF. The calorimeter would cost roughly 3M CHF. The readout electronics could be quite expensive when high-quality digitizers have to be foreseen for the calorimeter. Positron tracking detectors will probably not contribute significantly.

A price tag of 10M CHF seems justified if compared with the preliminary MECO budget, which is three times larger. The MECO collaboration presently consists of seven institutions and 30 physicists, but may have to be enlarged considerably.

manpower

The sizes of the groups are listed in Table VI. We feel confident that the available manpower should be enough to finish the experiment within the time period discussed above.

TABLE VI. Manpower

Institution	physicists		
PSI	5		
Zurich	5		
Switzerland		10	
Pavia	3		
Pisa	7		
Roma	2		
Italy		12	
KEK	5		
Tokyo	5		
Waseda	4		
Japan		14	
JINR	5		
Swierk	4		
Tbilisi	4		
others		13	
total			48

[1] J.D. Vergados, Phys. Rep. **133**, 1 (1986).
[2] A. van der Schaaf, in *Progress in Particle and Nuclear Physics*, edited by A. Faessler, Vol. 31, p. 1, (Pergamon, Oxford, 1993).
[3] P. Depommier and C. Leroy, Rep. Prog. Phys. **58**, 61 (1995).
[4] R. Barbieri and L.J. Hall, Phys. Lett. **B338** (1994) 212;
R. Barbieri, L.J. Hall, and A. Strumia, Nucl. Phys. **B445** (1995) 219.
[5] MECO Collaboration,
W. Molzon spokesman, *A Search for $\mu^- N \rightarrow E^- N$ with Sensitivity Below* 10^{-16}, AGS proposal P940, 1997.
[6] R. Mischke, presented at the *International Workshop on JHF Science*, Tsukuba, Japan, March 3–7, 1998.
[7] R.M. Barnett *et al.*, Phys. Rev. **D54**, 1 (1996) and 1997 off-year partial update for the 1998 edition.
[8] SINDRUM II Collaboration, submitted to Phys.Rev.C, 1998.
[9] K. Jungmann, presented at the *International Workshop on JHF Science*, Tsukuba, Japan, March 3–7, 1998.
[10] T. Kirk, presented at the *International Workshop on JHF Science*, Tsukuba, Japan, March 3–7, 1998.
[11] L.J. Hall, V.A. Kostelechy and S. Raby, Nucl. Phys. **B267** (1986) 415.
[12] J. Hisano, T. Moroi, K. Tobe and M. Yamaguchi, Phys. Lett. **B391** (1997) 341.
[13] J. Hisano, D. Nomura, T. Yanagida, KEK Preprint KEK-TH-548, November, 1997 (hep-ph/9711348).
[14] J. Hisano, T. Moroi, K. Tobe, M. Yamaguchi, and T. Yanagida, Phys. Lett. **B357** (1995) 579.
[15] M. Chaichian, K.Huitu, Phys. Lett. **B384** (1996) 157.
[16] Y. Kuno and Y. Okada, Phys. Rev. Lett. **77** (1996) 434.
[17] Y. Kuno, A. Maki, and Y. Okada, Phys. Rev. D55 (1997) 2517.
[18] Y. Kuno, Internal report.
[19] A. Badertscher, D. Renker and L. Simons, PSI internal report (1989).
[20] T. Doke, Nucl. Instr. and Meth. **A327** (1993) 113–118.
[21] A. Hitachi *et al.*, Phys. Rev. **B27** (1983) 5279.
[22] R6041Q, Hamamatsu Photonics K.K.